Supplementary Information:

Analytical van der Waals interaction potential for faceted nanoparticles

Brian Hyun-jong Lee and Gaurav Arya*

Department of Mechanical Engineering and Material Science,
Duke University, Durham, NC 27708, USA

E-mail: gaurav.arya@duke.edu

Detailed derivation of the vdW potential

Distance between interacting facets

The interacting facet of particle P2, denoted by F2, can be described as a plane passing through three of its vertices $\mathbf{v_1} = [x_{\mathrm{v1}}, y_{\mathrm{v1}}, z_{\mathrm{v1}}]$, $\mathbf{v_2} = [x_{\mathrm{v2}}, y_{\mathrm{v2}}, z_{\mathrm{v2}}]$, and $\mathbf{v_3} = [x_{\mathrm{v3}}, y_{\mathrm{v3}}, z_{\mathrm{v3}}]$, as shown in Fig. S1a. The normal vector $\mathbf{n}$ of the plane can be obtained by the cross product of the two vectors $\mathbf{L_1} = \mathbf{v_2} - \mathbf{v_1}$ and $\mathbf{L_2} = \mathbf{v_3} - \mathbf{v_1}$ formed by the three points:

$$\begin{aligned} \mathbf{n} = \mathbf{L_1} \times \mathbf{L_2} &= [n_{\mathrm{x}}, n_{\mathrm{y}}, n_{\mathrm{z}}] \\ n_{\mathrm{x}} &= (y_{\mathrm{v2}} - y_{\mathrm{v1}})(z_{\mathrm{v3}} - z_{\mathrm{v1}}) - (z_{\mathrm{v2}} - z_{\mathrm{v1}})(y_{\mathrm{v3}} - y_{\mathrm{v1}}) \\ n_{\mathrm{y}} &= (z_{\mathrm{v2}} - z_{\mathrm{v1}})(x_{\mathrm{v3}} - x_{\mathrm{v1}}) - (x_{\mathrm{v2}} - x_{\mathrm{v1}})(z_{\mathrm{v3}} - z_{\mathrm{v1}}) \\ n_{\mathrm{z}} &= (x_{\mathrm{v2}} - x_{\mathrm{v1}})(y_{\mathrm{v3}} - y_{\mathrm{v1}}) - (y_{\mathrm{v2}} - y_{\mathrm{v1}})(x_{\mathrm{v3}} - x_{\mathrm{v1}}). \end{aligned} \tag{1}$$

The equation of plane for F2 is then given by

$$n_{\mathrm{x}}(x - x_{\mathrm{v1}}) + n_{\mathrm{y}}(y - y_{\mathrm{v1}}) + n_{\mathrm{z}}(z - z_{\mathrm{v1}}) = 0, \tag{2}$$

where (x, y, z) represents the position of an arbitrary point on this plane. To obtain the distance d_x between the interacting facets of particles P1 and P2 in x axis, we note that: (i) the center of mass of P1 is located at the origin and axis-aligned with the Cartesian coordinate such that its interacting face points along the $+x$ direction, and (ii) d_x is defined as the distance between the centers of the surface atoms of the interacting facets (Fig. S1b). Given that the interacting facet of P1 is offset by a distance $D/2$ from the origin (half the particle dimension along the x-axis) and the size of the atoms making of the particles is σ, $d_x = x - \frac{D}{2} + \sigma$, which, combined with Eq. 2, yields the final form of d_x given by

$$d_x = c_1 y + c_2 z + c_3 \tag{3}$$

where $c_1 = -n_y/n_x$, $c_2 = -n_z/n_x$, and $c_3 = x_{\mathrm{v1}} - D/2 + \sigma - c_1 y_{\mathrm{v1}} - c_2 z_{\mathrm{v1}}$.

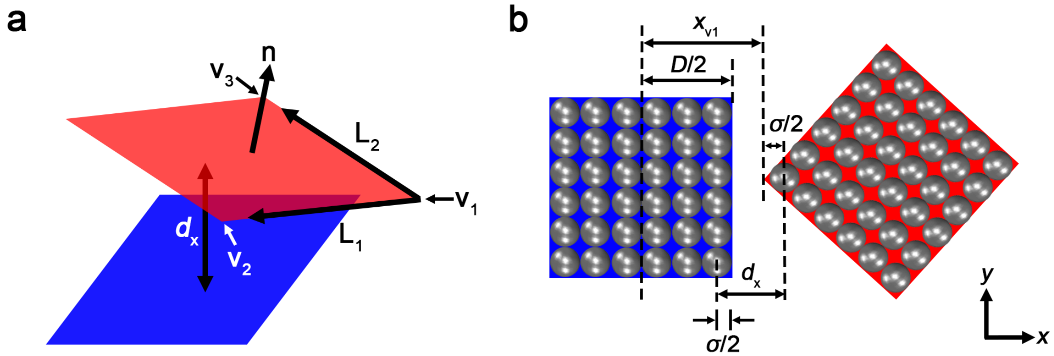

Figure S1: (a) Interacting facets of particles P1 (blue) and P2 (red). (b) x-y projection of P1 and P2. The center of mass of P1 is at the origin.

Analytical solutions to the energy integral

The energy integral for a given region r and given power-law component of the rod potential with coefficient C_ν and scaling exponent n_ν is given by

$$U_{\mathrm{vdW}}^{\nu,r} = \gamma C_\nu \int_{y_{r,1}}^{y_{r,2}} \int_{z_{r,1}(y)}^{z_{r,2}(y)} \left(\frac{\sigma}{d_{r,x}(y,z)}\right)^{n_\nu} dz\, dy. \tag{4}$$

Substituting Eq. 3 specific for region r along with its z-integral limits $z_{r,1} = b_{r,1}y + a_{r,1}$ and $z_{r,2} = b_{r,2}y + a_{r,2}$ into Eq. 4, we obtain

$$U_{\mathrm{vdW}}^{\nu,r} = \gamma C_\nu \sigma^{n_\nu} \int_{y_{r,1}}^{y_{r,2}} \int_{b_{r,1}y+a_{r,1}}^{b_{r,2}y+a_{r,2}} (c_{r,1}y + c_{r,2}z + c_{r,3})^{-n_\nu}\, dz\, dy. \tag{5}$$

Case 1. We first consider the most general case where d_x is a function of y and z, i.e., $c_{r,1} \neq 0$ and $c_{r,2} \neq 0$. For this case, the solution to the inner integral with respect to z is given by

$$\begin{aligned} U_{\mathrm{vdW}}^{\nu,r} = \frac{\gamma C_\nu \sigma^{n_\nu}}{c_{r,2}(n_\nu - 1)} \int_{y_{r,1}}^{y_{r,2}} & \left[a_{r,1}c_{r,2} + c_{r,3} + (c_{r,1} + b_{r,1}c_{r,2})y\right]^{1-n_\nu} \\ & - \left[a_{r,2}c_{r,2} + c_{r,3} + (c_{r,1} + b_{r,2}c_{r,2})y\right]^{1-n_\nu}\, dy, \end{aligned} \tag{6}$$

The solution to this outer integral depends on the values of $c_{r,1}$, $c_{r,2}$, $b_{r,1}$, and $b_{r,2}$.

Case 1A. When $c_{r,1} + b_{r,1}c_{r,2} \neq 0$ and $c_{r,1} + b_{r,2}c_{r,2} \neq 0$, the solution is given by

$$\begin{aligned} U_{\mathrm{vdW}}^{\nu,r} &= \frac{\gamma C_\nu \sigma^{n_\nu}}{c_{r,2}(n_\nu - 1)(n_\nu - 2)} \\ &\times \Bigg\{ \frac{\left[a_{r,1}c_{r,2} + c_{r,3} + (c_{r,1} + b_{r,1}c_{r,2})y_{r,1}\right]^{2-n_\nu} - \left[a_{r,1}c_{r,2} + c_{r,3} + (c_{r,1} + b_{r,1}c_{r,2})y_{r,2}\right]^{2-n_\nu}}{(c_{r,1} + b_{r,1}c_{r,2})} \\ &+ \frac{\left[a_{r,2}c_{r,2} + c_{r,3} + (c_{r,1} + b_{r,2}c_{r,2})y_{r,2}\right]^{2-n_\nu} - \left[a_{r,2}c_{r,2} + c_{r,3} + (c_{r,1} + b_{r,2}c_{r,2})y_{r,1}\right]^{2-n_\nu}}{(c_{r,1} + b_{r,2}c_{r,2})} \Bigg\}. \end{aligned} \tag{7}$$

This equation is equivalent to the solution to the $d_x \equiv d_x(y,z)$ case provided in Table 1.

Case 1B. However, when $c_{r,1} + b_{r,1}c_{r,2} = 0$,

$$\begin{aligned} U_{\mathrm{vdW}}^{\nu,r} &= \frac{\gamma C_\nu \sigma^{n_\nu}}{c_{r,2}(n_\nu - 1)(n_\nu - 2)} \Bigg\{ (y_{r,2} - y_{r,1})(a_{r,1}c_{r,2} + c_{r,3})^{1-n_\nu} \\ &+ \frac{\left[a_{r,2}c_{r,2} + c_{r,3} + (c_{r,1} + b_{r,2}c_{r,2})y_{r,2}\right]^{2-n_\nu} - \left[a_{r,2}c_{r,2} + c_{r,3} + (c_{r,1} + b_{r,2}c_{r,2})y_{r,1}\right]^{2-n_\nu}}{(c_{r,1} + b_{r,2}c_{r,2})} \Bigg\}. \end{aligned} \tag{8}$$

Case 1C. When $c_{r,1} + b_{r,2}c_{r,2} = 0$,

$$U^{\nu,r}_{\mathrm{vdW}} = \frac{\gamma C_\nu \sigma^{n_\nu}}{c_{r,2}(n_\nu - 1)(n_\nu - 2)} \Big\{ (y_{r,1} - y_{r,2})(a_{r,2}c_{r,2} + c_{r,3})^{1-n_\nu}$$
$$+ \frac{\big[a_{r,1}c_{r,2} + c_{r,3} + (c_{r,1} + b_{r,1}c_{r,2})y_{r,1}\big]^{2-n_\nu} - \big[a_{r,1}c_{r,2} + c_{r,3} + (c_{r,1} + b_{r,1}c_{r,2})y_{r,2}\big]^{2-n_\nu}}{(c_{r,1} + b_{r,1}c_{r,2})} \Big\}. \tag{9}$$

Case 1D. Finally, when $c_{r,1} + b_{r,2}c_{r,2} = c_{r,1} + b_{r,1}c_{r,2} = 0$,

$$U^{\nu,r}_{\mathrm{vdW}} = \frac{\gamma C_\nu \sigma^{n_\nu}}{c_{r,2}(n_\nu - 1)(n_\nu - 2)}$$
$$\times \Big\{ (y_{r,2} - y_{r,1})(a_{r,1}c_{r,2} + c_{r,3})^{1-n_\nu} + (y_{r,1} - y_{r,2})(a_{r,2}c_{r,2} + c_{r,3})^{1-n_\nu} \Big\}. \tag{10}$$

Case 2. The solution to the energy integral exhibits different forms when the distance between the facets are not a function of both y and z. When $c_{r,2} = 0$ and $d_x = d_x(y)$, the integral reduces to

$$U^{\nu,r}_{\mathrm{vdW}} = \gamma C_\nu \sigma^{n_\nu} \int_{y_{r,1}}^{y_{r,2}} \int_{b_{r,1}y + a_{r,1}}^{b_{r,2}y + a_{r,2}} (c_{r,1}y + c_{r,3})^{-n_\nu} \, dz \, dy$$
$$= \gamma C_\nu \sigma^{n_\nu} \int_{y_{r,1}}^{y_{r,2}} (b_{r,2}y + a_{r,2} - b_{r,1}y - a_{r,1})(c_{r,1}y + c_{r,3})^{-n_\nu} \, dy \tag{11}$$

with a solution given by

$$U^{\nu,r}_{\mathrm{vdW}} = \frac{\gamma C_\nu \sigma^{n_\nu}}{c_{r,1}^2 (n_\nu - 2)(n_\nu - 1)}$$
$$\times \Big\{ (c_{r,1}y_{r,2} + c_{r,3})^{1-n_\nu} \big[(a_{r,1} - a_{r,2})c_{r,1}(n_\nu - 2) + (b_{r,1} - b_{r,2})(c_{r,3} + c_{r,1}(n_\nu - 1)y_{r,2} \big]$$
$$-(c_{r,1}y_{r,1} + c_{r,3})^{1-n_\nu} \big[(a_{r,1} - a_{r,2})c_{r,1}(n_\nu - 2) + (b_{r,1} - b_{r,2})(c_{r,3} + c_{r,1}(n_\nu - 1)y_{r,1}) \big] \Big\}. \tag{12}$$

This equation is equivalent to the solution for the $d_x \equiv d_x(y)$ case provided in Table 1.

Case 3. When $c_{r,1} = 0$ and $d_x = d_x(z)$, the energy integral reduces to

$$U^{\nu,r}_{\mathrm{vdW}} = \gamma C_\nu \sigma^{n_\nu} \int_{y_{r,1}}^{y_{r,2}} \int_{b_{r,1}y + a_{r,1}}^{b_{r,2}y + a_{r,2}} (c_{r,2}z + c_{r,3})^{-n_\nu} \, dz \, dy$$
$$= \frac{\gamma C_\nu \sigma^{n_\nu}}{c_{r,2}(1 - n_\nu)} \int_{y_{r,1}}^{y_{r,2}} \Big[(a_{r,2}c_{r,2} + c_{r,3} + b_{r,2}c_{r,2}y)^{1-n_\nu} - (a_{r,1}c_{r,2} + c_{r,3} + b_{r,1}c_{r,2}y)^{1-n_\nu} \Big] \, dy. \tag{13}$$

The solution depends on the values of $b_{r,1}$ and $b_{r,2}$.

Case 3A. When $b_{r,1} \neq 0$ and $b_{r,2} \neq 0$,

$$U^{\nu,r}_{\text{vdW}} = \frac{\gamma C_\nu \sigma^{n_\nu}}{c_{r,2}(1-n_\nu)} \left\{ \frac{(a_{r,2}c_{r,2} + c_{r,3} + b_{r,2}c_{r,2}y_{r,2})^{2-n_\nu} - (a_{r,2}c_{r,2} + c_{r,3} + b_{r,2}c_{r,2}y_{r,1})^{2-n_\nu}}{b_{r,2}c_{r,2}(2-n_\nu)} \right. \\ \left. + \frac{(a_{r,1}c_{r,2} + c_{r,3} + b_{r,1}c_{r,2}y_{r,1})^{2-n_\nu} - (a_{r,1}c_{r,2} + c_{r,3} + b_{r,1}c_{r,2}y_{r,2})^{2-n_\nu}}{b_{r,1}c_{r,2}(2-n_\nu)} \right\}. \tag{14}$$

This is equivalent to the solution to the $d_x \equiv d_x(z)$ case provided in Table 1.

Case 3B. When $b_{r,2} = 0$,

$$U^{\nu,r}_{\text{vdW}} = \frac{\gamma C_\nu \sigma^{n_\nu}}{c_{r,2}(1-n_\nu)} \left\{ (y_{r,2} - y_{r,1})(a_{r,2}c_{r,2} + c_{r,3})^{1-n_\nu} \right. \\ \left. + \frac{(a_{r,1}c_{r,2} + c_{r,3} + b_{r,1}c_{r,2}y_{r,1})^{2-n_\nu} - (a_{r,1}c_{r,2} + c_{r,3} + b_{r,1}c_{r,2}y_{r,2})^{2-n_\nu}}{b_{r,1}c_{r,2}(2-n_\nu)} \right\}. \tag{15}$$

Case 3C. When $b_{r,1} = 0$,

$$U^{\nu,r}_{\text{vdW}} = \frac{\gamma C_\nu \sigma^{n_\nu}}{c_{r,2}(1-n_\nu)} \left\{ (y_{r,1} - y_{r,2})(a_{r,1}c_{r,2} + c_{r,3})^{1-n_\nu} \right. \\ \left. + \frac{(a_{r,2}c_{r,2} + c_{r,3} + b_{r,2}c_{r,2}y_{r,2})^{2-n_\nu} - (a_{r,2}c_{r,2} + c_{r,3} + b_{r,2}c_{r,2}y_{r,1})^{2-n_\nu}}{b_{r,2}c_{r,2}(2-n_\nu)} \right\}. \tag{16}$$

Case 3D. Lastly, when $b_{r,2} = b_{r,1} = 0$,

$$U^{\nu,r}_{\text{vdW}} = \frac{\gamma C_\nu \sigma^{n_\nu}}{c_{r,2}(1-n_\nu)} \Big[(y_{r,2} - y_{r,1})(a_{r,2}c_{r,2} + c_{r,3})^{1-n_\nu} + (y_{r,1} - y_{r,2})(a_{r,1}c_{r,2} + c_{r,3})^{1-n_\nu} \Big]. \tag{17}$$

Case 4. Finally, when the facets are parallel ($c_{r,1} = c_{r,2} = 0$), the solution to the energy integral is given by

$$U^{\nu,r}_{\text{vdW}} = \gamma C_\nu \sigma^{n_\nu} \int_{y_{r,1}}^{y_{r,2}} \int_{b_{r,1}y + a_{r,1}}^{b_{r,2}y + a_{r,2}} c_{r,3}^{-n_\nu} \, dz \, dy \\ = \frac{\gamma C_\nu \sigma^{n_\nu}}{2c_{r,3}^{n_\nu}} (y_{r,2} - y_{r,1})[(y_{r,2} + y_{r,1})(b_{r,2} - b_{r,1}) + 2(a_{r,2} - a_{r,1})] \tag{18}$$

This is equivalent to the solution to the constant d_x case provided in Table 1.

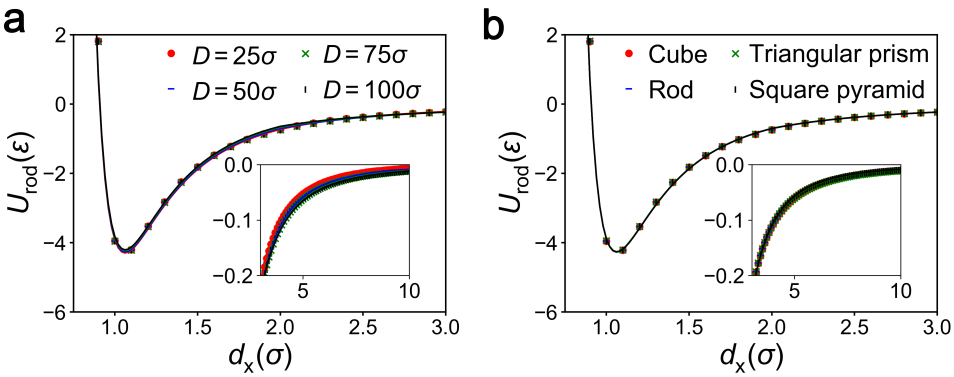

Figure S2: Power-law model for the rod potential U_{rod} of: (a) nanocubes of varying sizes D, and (b) faceted particles of varying shapes of size $D = 50\sigma$. Inset shows a zoomed view of the long-ranged portion of the potential. Symbols represent energies computed from atomistic summation and solid lines represent power-law fits.

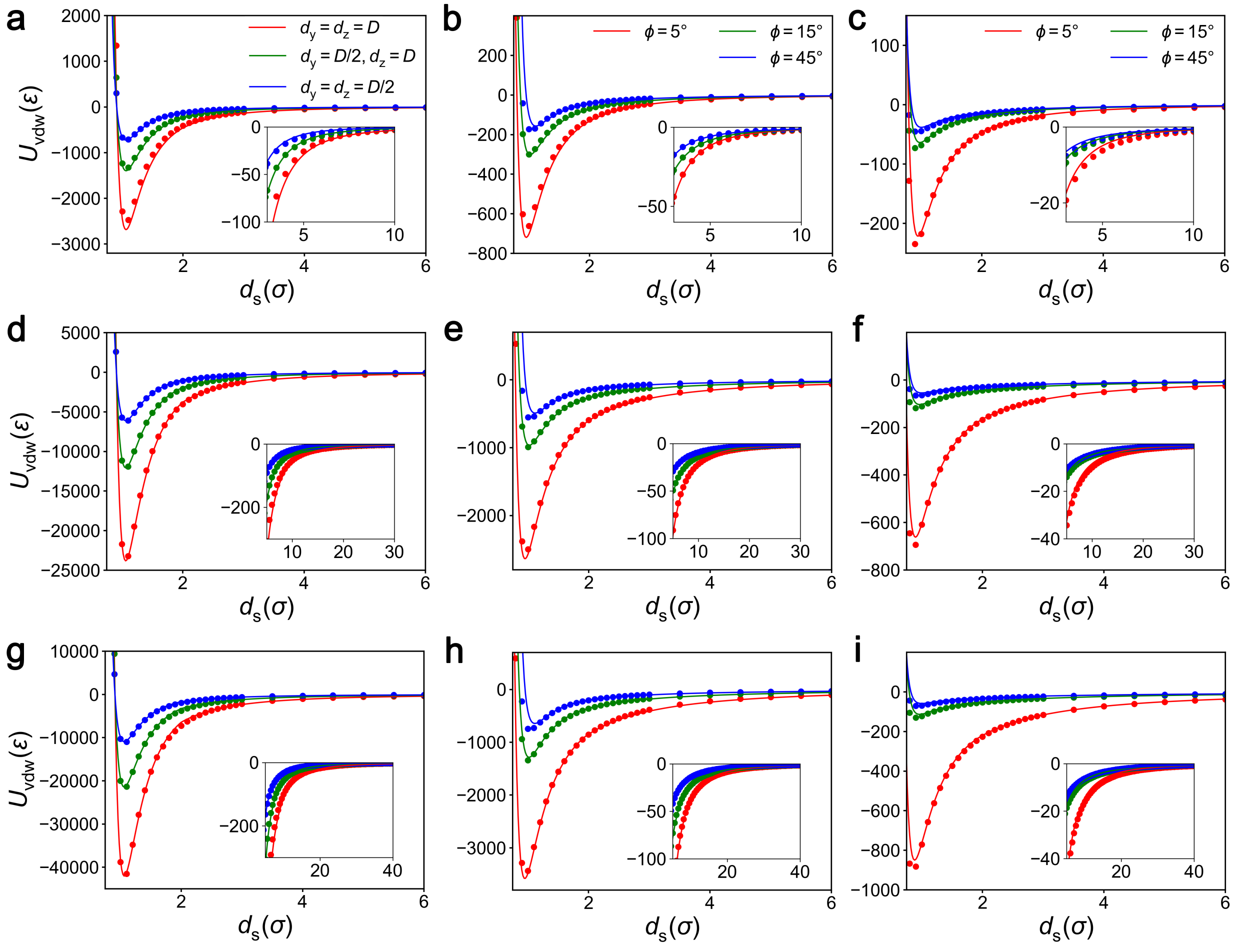

Figure S3: Comparison of U_{vdW} calculated from the analytical model (solid lines) and from atomistic summation (symbols) for $D = 25\sigma$ (a–c), $D = 75\sigma$ (d–f), and $D = 100\sigma$ (g–i) nanocubes. The plots correspond to: (a,d,g) parallel configurations ($\phi = \theta = \psi = 0°$), (b,e,h) coplanar configurations ($\theta = \psi = 0°$, $d_y = 0.5D$, $d_z = D$), and (c,f,i) general configurations ($\phi = \theta = \psi$, $d_y = d_z = 0.5D$). The legends in (a), (b), (c) also apply to (d,g), (e,h), and (f,i), respectively.

Application to specific materials.

In this study, we employed the Lennard Jones (LJ) potential to model van der Waals (vdW) interaction energy between atoms in which σ represents the diameter of the atoms and ε represents the interatomic energy parameter. While we have not specified the values of ε and σ to make the model applicable to arbitrary materials, careful choice of these LJ parameters is essential for application of the analytical model to experimental nanoparticles made of specific materials. The MATLAB application provides two methods for inputting the values of ε and σ. The first method involves the user directly inputting the desired parameters. This option is chosen by the application if the input value of ε in the edit field is not equal to 0 (see Fig. 7 of the main manuscript). For the second method, the user needs to provide the literature values of the relevant material properties, including the Hamaker constant (A), atomic diameter (σ), atomic mass (m), and the mass density (ρ). From these material

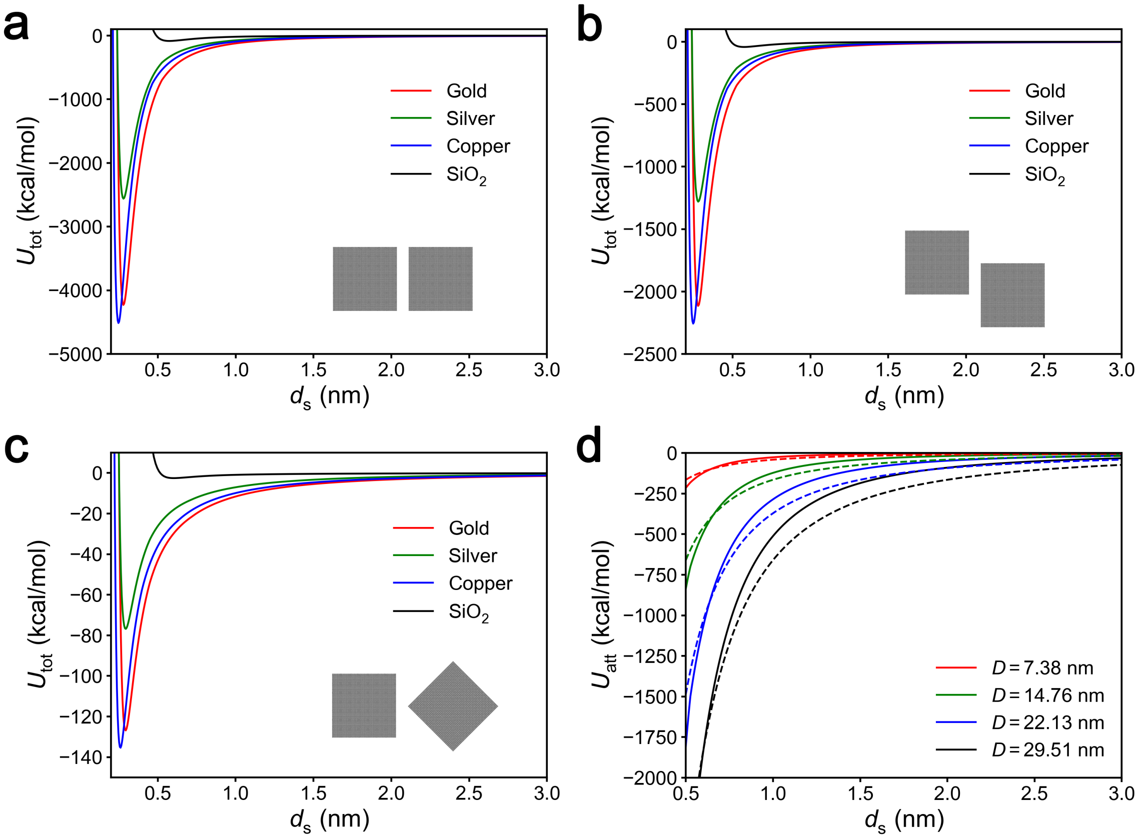

Figure S4: Application of the analytical model to specific materials. (a-c) U_{tot} between two nanocubes with varying materials. The size of the nanocubes are kept at $D = 50\sigma$ and the configurations are (a) face-face ($d_y = d_z = D$, $\phi = \theta = \psi = 0°$), (b) parallel nanocubes with half of their faces overlapping ($d_y = D/2$, $d_z = D$, $\phi = \theta = \psi = 0°$), (c) coplanar, face-edge ($d_y = D/2$, $d_z = D$, $\phi = 45°$, $\theta = \psi = 0°$) configurations. (d) Comparison of U_{att} obtained from the analytical model (solid lines) and the experimentally derived energies (dashed lines) for gold nanocubes with varying side lengths (D).

properties, ε is derived through the following relationship, $\varepsilon = \frac{Am^2}{4\pi^2\rho^2(2^{(1/6)}\sigma)^6}$ [1]. This method is chosen when the inputted value of ε is equal to 0.

Table S1: LJ parameters for selected materials

Material	A **(J)**	m **(Da)**	ρ **(g/cm^3)**	σ **(nm)**	ε **(kcal/mol)**
Gold	2.5×10^{-19} [2]	197.0	19.3	0.263 [3]	0.396
Silver	1.5×10^{-19} [4]	107.9	10.5	0.263 [3]	0.240
Copper	2.7×10^{-19} [5]	63.55	8.96	0.233 [3]	0.423
SiO_2	7.6×10^{-20} [6]	60.08	2.65	0.54 [7]	0.0079

All values of m and ρ are taken from [8].

To demonstrate the application of the model to specific materials, we have computed the vdW interaction energies between nanocubes made of gold, silver, copper, and SiO_2. The parameters used for these materials are given in Table S1. For SiO_2, we have employed an approximate, coarse-grained model in which each SiO_2 molecule is represented as a single pseudo atom. We have also assumed that the molecules are in crystalline arrangements, with σ chosen to equal its lattice constant [7]. The results shown in Figure S7a-c demonstrate that the depths and the locations of the energy wells vary significantly depending on the material properties of the nanocubes. Gold and copper nanocubes are interacting with significant interaction strengths while the SiO_2 nanocubes are weakly interacting.

To validate the accuracy of the model in its application to specific materials, we have compared the attractive portions of the vdW energies (U_{att}) obtained from our analytical model with those obtained from the atomic force microscopy (AFM). AFM experiments have shown that the vdW interaction energies between gold surfaces in water can be described by the expression [2],

$$E_{\text{A}}(d_{\text{s}}) = -\frac{A}{12\pi d_{\text{s}}^2} \tag{19}$$

where, E_{A} and d_{s} are the energy per unit area and the surface separation distances. Experiments approximated the vdW interaction energies between gold surfaces with $A = 2.5 \times 10^{-19}$ J. While Eq. 19 was derived assuming that the two surfaces are infinite and parallel, it can be used to roughly estimate the vdW interaction energies of two nanocubes in face-face configurations when the surfaces are close to each other. The results depicted in Figure S7d demonstrate that the energies obtained from the analytical model agree well with the experimentally-derived energies, especially when the nanocubes are close to each other. Such agreement further supports the effectiveness of our model in accurately obtaining the vdW energy between the nanocubes.

Computational implementation of model

In implementing the model, we consider the nanocubes to be in P1's frame of reference so that P1 is at the origin with its faces aligned normal to the three axes and P2 is interacting with P1's face along the positive x-axis. We then proceed to determine the positions of the 8 vertices of P2, from which we identify the vertex or set of vertices exhibiting the smallest x values, i.e., closest to the interacting face of P1; we denote these vertices as "adjoining vertices". Depending on the identity and the number of such vertices, we identify all interacting faces of P2. For example, if there are four adjoining vertices, we know that the cubes are parallel and there is one interacting face. Two adjoining vertices would imply that one edge of P2 is parallel to P1's face and that there are two interacting faces. The most general case is when there is a single adjoining vertex and three faces of P2 are interacting. After identification of P2's interacting faces, we segment each such face into regions of constant y integral limits and linear $z(y)$ integral limits, as illustrated for a representative interacting face in Fig. 1h of the main manuscript. Ideally, the regions need to be further segmented so that the d_{x} of all rods are either greater or less than d_{cut} in each subregion. However, we chose the set of rod potential parameters C_ν and n_ν based on d_{s} of the particle and not the d_{x} of each rod for two reasons. First, when $d_{\mathrm{s}} > d_{\mathrm{cut}}$, d_{x} of all of the rods are greater than d_{cut} and further segmentation of the regions are unnecessary. Second, when $d_{\mathrm{s}} < d_{\mathrm{cut}}$, U_{vdW} is dominated by the interaction energies of the rods that are closest to P1, as demonstrated in Fig. 5b. Therefore, our simplification for determining power-law parameters based on d_{s} is quite reasonable.

While most aspects of the analytical model can be straightforwardly implemented, computationally segmenting the interacting faces into regions sharing common upper and lower integral limit functions $z(y)$ is not simple. To achieve this task, we recognize that the function $z(y)$ can change its form at y values corresponding to any one of the following: y-boundaries of P1, vertex positions of P2, or intersection points of P2's edges with P1's z-boundaries.

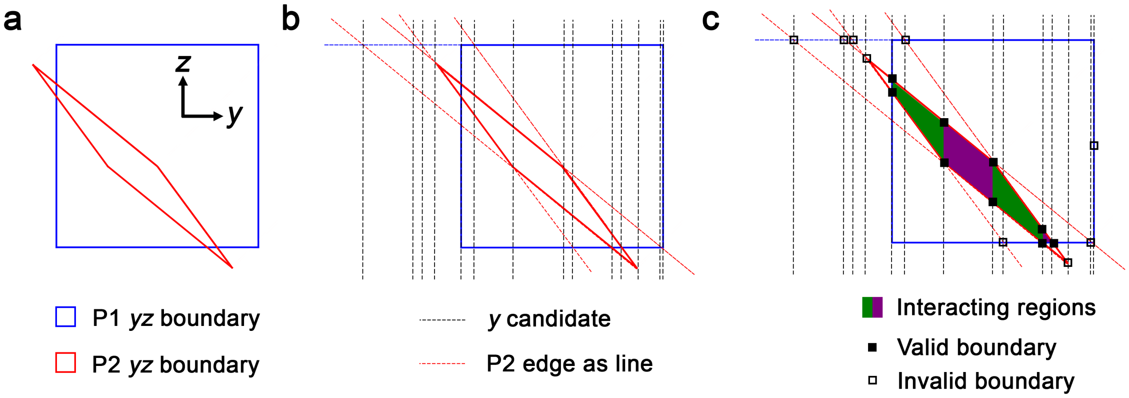

Figure S5: Computational algorithm for region segmentation: (a) F_1 y-z boundaries from Fig. 1g. (b) Determination of all possible y values (dashed lines) at which the integral limit $z(y)$ may change its form. (c) Evaluation of y candidates that are within the intersection of P1 and P2 boundaries (solid symbols) to obtain the interaction regions with equivalent integral limits.

Therefore, for each interacting facet of P2 identified, such as the one depicted in Fig. S4a for illustration, we save all y values that meet the above criteria within an array $\mathbf{y}_{\text{candidate}}$. For the intersection of P2's edges with P1's z-boundaries, we treat P2's edges as continuous lines and use their corresponding line equations to determine where the lines cross P1's z-boundaries. The array members of $\mathbf{y}_{\text{candidate}}$ obtained for our illustrative example are marked in Fig. S4b. We then sort the array in ascending order and identify the valid boundaries by evaluating whether each array member falls within the intersection area of the P1 and P2 y-z boundaries, as shown in Fig. S4c. In this manner, we are able to divide P2's interacting faces into a set of regions bounded by four straight lines, two in the y direction with fixed y values and two in the z direction that vary linearly with y coordinate.

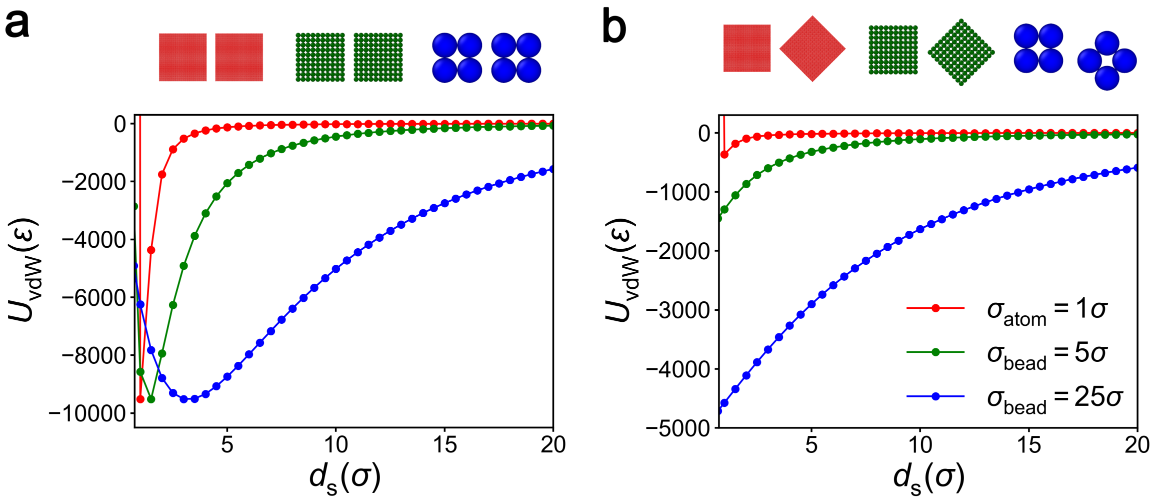

Figure S6: Comparison of the vdW energy landscape U_{vdW} of atomistic nanocubes of size $D = 50\sigma$ and coarse-grained (CG) models of nanocubes of the same size at two different levels of coarse-graining. The nanocubes are in (a) face-face configuration ($\phi = \theta = \psi = 0^\circ$ and $d_y = d_z = D$), and (b) face-edge configuration ($\phi = 45^\circ$, $\theta = \psi = 0^\circ$ and $d_y = D/2$ and $d_z = D$). The atomistic cubes were constructed out of a $50 \times 50 \times 50$ cubic lattice of atoms of size 1σ. The two CG models were constructed out of $10 \times 10 \times 10$ and $2 \times 2 \times 2$ cubic lattices of beads of size 5σ and 25σ, respectively. The Lennard-Jones energy parameter for atoms was set to ε, while that of the CG beads were scaled to match the minima of U_{vdW} of the atomistic cubes in the face-face configurations. The CG models, even the finer one, are clearly unable to capture the distance-scaling of the vdW energy (a) as well as its orientational dependence (b).

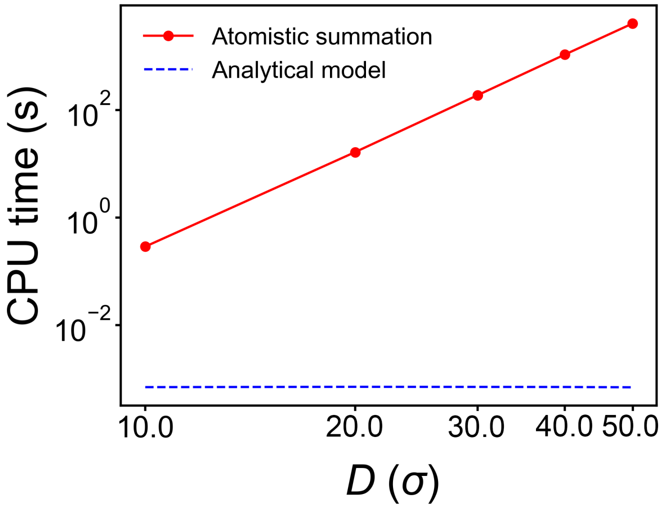

Figure S7: Comparison between atomistic summation and analytical model of CPU times required for carrying out a single vdW interaction energy evaluation for nanocubes of varying sizes. Both methods were implemented in MATLAB on an Intel Core i7-7700 processor, and the CPU time was measured using the *timeit* function in MATLAB. The CPU time for the atomistic summation method rose rapidly with cube side length (D) as $\approx 2.6 \times 10^{-7} D^{6}$ seconds per evaluation, whereas the analytical model exhibited constant CPU time of $\approx 7 \times 10^{-4}$ seconds.

References

(1) Israelachvili, J. N. *Intermolecular and Surface Forces*; Academic press, 2015.

(2) Biggs, S.; Mulvaney, P. Measurement of the forces between gold surfaces in water by atomic force microscopy. *J. Chem. Phys.* **1994**, *100*, 8501–8505.

(3) Heinz, H.; Vaia, R.; Farmer, B.; Naik, R. Accurate simulation of surfaces and interfaces of face-centered cubic metals using 12- 6 and 9- 6 Lennard-Jones potentials. *J. Phys. Chem. C* **2008**, *112*, 17281–17290.

(4) Bell, N.; Dimos, D. Calculation of Hamaker Constants in Nonaqueous Fluid Media. *Mater. Res. Soc. Proc.* **2000**, *624*.

(5) Eichenlaub, S.; Chan, C.; Beaudoin, S. P. Hamaker constants in integrated circuit metalization. *J. Colloid Interface Sci.* **2002**, *248*, 389–397.

(6) Bergström, L. Hamaker constants of inorganic materials. *Adv. Colloid Interface Sci.* **1997**, *70*, 125–169.

(7) Will, G.; Bellotto, M.; Parrish, W.; Hart, M. Crystal structures of quartz and magnesium germanate by profile analysis of synchrotron-radiation high-resolution powder data. *J. Appl. Crystallogr.* **1988**, *21*, 182–191.

(8) Haynes, W. M. *CRC handbook of chemistry and physics*; CRC press, 2014.